Journal of Applied Electrochemistry **30**: 607–615, 2000.

Application of EIS to the initial stages of atmospheric zinc corrosion

S.C. CHUNG[1], S.L. SUNG[1], C.C. HSIEN[2] and H.C. SHIH[1]*
[1]*Department of Materials Science and Engineering, National Tsing Hua University, Hsinchu 300, Taiwan, R.O.C;*
[2]*Materials Research Laboratories, Industrial Technology Research Institute, Chutung, Hsinchu 310, Taiwan, R.O.C*
*(*author for correspondence, fax: +886-3-5710290, e-mail: hcshih@mse.nthu.edu.tw)*

Received 15 February 1999; accepted in revised form 22 December 1999

Key words: atmospheric corrosion, EIS, initial stage, zinc

Abstract

This paper reports an experimental study of the initial stage of atmospheric zinc corrosion using *ex situ* electrochemical impedance spectroscopy (EIS) in methanol electrolyte. Compared with the traditional techniques for studying atmospheric corrosion, such as gravimetry, the EIS technique significantly reduced the exposure time for detectable corrosion at any relative humidity from several days to a few hours. The samples were first exposed to synthetic atmospheres with careful control of O_2 and CO_2 concentrations, relative humidity and temperature. EIS was then used to measure the polarization resistance (R_p) of the exposed samples. The corrosion products were analysed by a combination of grazing-angle X-ray diffraction, Fourier transform infrared spectroscopy and photoelectron spectroscopy. Several interesting phenomena occurring in the initial stage of corrosion were demonstrated by studying the electrochemical properties of the surface layer formed on the zinc. At high values of relative humidity (RH 95–100%), with $CO_2 > 40$ ppm, the R_p of the surface film formed increased monotonically with time and relative humidity. At intermediate values of relative humidity (RH 50–85%) in the presence of CO_2 (40–500 ppm), R_p first increased with time, reached a maximum, then fell from the maximum value before again rising slowly. A brief description of the mechanism of atmospheric zinc corrosion is proposed.

1. Introduction

Zinc is extensively used for coating, or galvanizing, ferrous metal products. Many atmospheric corrosion studies have investigated the compositions of corrosion products formed on zinc for various exposure conditions, types and levels of pollutants, and wet–dry cycles [1–14]. Zinc specimens exposed to an unpolluted dry atmosphere were quickly covered with a thin grey layer of zincite, ZnO. When the relative humidity increases, zincite is replaced by a white compact corrosion product of zinc hydroxide, $Zn(OH)_2$, which forms the basis for further growth of corrosion products. Upon interaction with CO_2, zinc transforms into white rust, a complex hydrated zinc carbonate/zinc hydroxide [15–17]; that is, $Zn_5(CO_3)_2(OH)_6$ or $Zn_4CO_3(OH)_6H_2O$, as suggested by Odnevall et al. [3]. The latter compounds are important intermediates in the subsequent formation of other corrosion products. The formation of the hydroxy carbonate layer is a rapid process, in which a thin layer may be formed within minutes or hours [18].

Many field exposure studies and laboratory investigations have been carried out on atmospheric zinc corrosion under various controlled conditions. However, few of these have dealt with the initiation stages due to measurement difficulties. Previously, the atmospheric corrosion of metal has been mainly investigated using gravimetric methods. However, these gravimetric data lack structural information about the corrosion products. Mass changes due to the atmospheric corrosion in dry environments are also generally too small to be measured, especially in the initial stages. Recently, some electrochemical techniques have been applied to the *in situ* measurement of atmospheric corrosion, that is, potentiometry with the scanning Kelvin probe [19] and electrochemical impedance spectroscopy (EIS) [20–25]. These *in situ* electrochemical techniques proceed under a thin water layer adsorbed on the metal surface. The thickness of this surface water layer ranges from 1 mm to 10 μm and samples have to be exposed to 100% relative humidity (RH) to keep the thickness of the surface water layer constant [21]. In a previous model introduced by Tomashov [26], four mechanisms of atmospheric corrosion were proposed, the active mechanism depending on the thickness, x, of the moisture layer, as follows: 'dry atmospheric corrosion' ($x <$ 10 nm); 'moist atmospheric corrosion' (10 nm $< x <$ 1 μm); 'wet atmospheric corrosion' (1 μm $< x <$ 1 mm); and 'complete immersion' ($x >$ 1 mm). Although these *in situ* electrochemical techniques are applicable to the study of the mechanism of the initial stage of atmo-

spheric corrosion, they are restricted to 'wet atmospheric corrosion' exposed to high relative humidities [27] and by the precise nature of the experimental set-up.

In this study, *ex situ* EIS is used in a nonaqueous electrolyte of methanol to investigate atmospheric zinc corrosion. In a nonaqueous electrolyte, on the one hand, oxide formation is significantly limited by the nature of such media which usually contain only trace quantities of residual water or air [28]. On the other hand, in the presence of water, corrosion products are formed during the electrochemical measurement which may interfere with those formed during atmospheric exposure. Thus, in nonaqueous electrolytes, the electrochemical properties of the surface can be quantitatively detected no matter how slight the mass changes are.

The aim of this work is to study the protection conferred by corrosion products formed during the initial stages of the atmospheric corrosion as a function of the environmental factors, RH and CO_2 concentration.

2. Experimental details

Zinc sheets, 25 mm × 20 mm × 3 mm with 99.95% purity, were used in all experiments. Prior to exposure, the specimens were prepared by polishing in ethanol with SiC emery papers to 1200 mesh, ultrasonically cleaning in ethanol, and drying in an evacuated desiccator over silica gel. After exposure, the specimens were also stored in a desiccator prior to analysis.

Specimens were exposed in a 100 mm × 100 mm × 100 mm chamber to test atmospheres at 28 ± 1 °C with controlled CO_2 content and RH. The experimental set-up for atmospheric exposure is schematically illustrated in Figure 1. CO_2-free air was obtained by bubbling normal air through a 20% monoethanolamine bath to remove the CO_2. The concentration of CO_2 in the test atmosphere was controlled by adding a known amount of CO_2 into the chamber with a syringe. An aqueous glycerin solution with specific glycerin-water ratio, prepared in accordance with ASTM D5032-90, was introduced into the bottom of the chamber to control the RH of the atmosphere. The air in the exposure chamber was refreshed every 24 h. Assuming the CO_2 consumption rate estimated by Falk et al. [17] for the atmospheric corrosion of zinc, the amount of CO_2 in the test chamber was sufficient to maintain a near-constant concentration over a 24 h period.

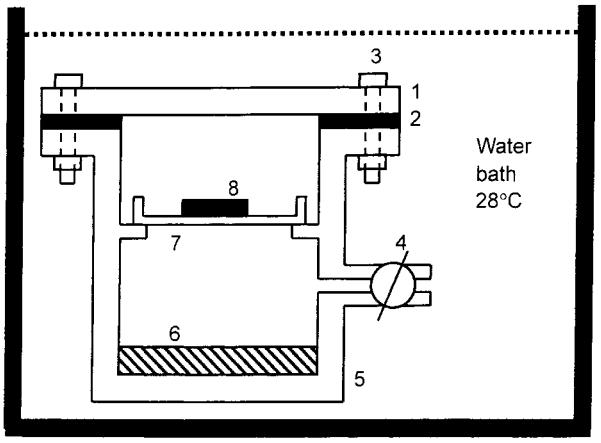

Fig. 1. A schematic diagram of the chamber for the atmospheric exposures: (1) upper cover, (2) rubber mat, (3) screws, (4) valve, (5) plexiglass chamber, (6) glycerin for relative humidity adjustment, (7) plastic bowl as specimen holder, and (8) zinc specimen.

Five different humidities (50, 70, 85, 95 and 100% RH) and five CO_2 concentrations (CO_2-free, 40, 350, 500 and 1000 ppm) were investigated. After exposure, the samples were analysed by EIS.

The electrochemical measurements were made using computer controlled measuring equipment, consisting of a potentiostat (EG&G 273) and a lock-in amplifier (EG&G 5301). Each component was connected to a personal computer via a parallel interface. The impedance measurements were carried out over the frequency range 40 mHz to 100 kHz and the amplitude of the applied voltage was 10 mV. The EIS was measured 5 min after each sample was immersed in the electrolyte.

A three-electrode cell was employed for the impedance measurements. A silver wire (1 mm dia.), with an electrochemically converted AgCl surface, served as reference electrode. This arrangement proved to have sufficient stability over the timescale of the experiments. The working electrode, of 1 cm^2 exposed area, was positioned parallel to a platinum flat sheet counter electrode. The specimens were dried in vacuum down to 10^{-1} torr for 5 min to remove the excess water layer adsorbed on the surface, then exposed to dry Ar gas, and finally were immersed in the test solution under an inert gas atmosphere. The electrolyte of pure methanol (<0.03% H_2O), used in all experiments, was doped with 0.003 M LiCl. The presence of chloride ions established a reversible Ag/AgCl half-cell electrode ($E_{Ag/AgCl(Cl^- \equiv 0.003\,M)}$) of 0.377 V vs SHE [29]. All potentials quoted with respect to the standard hydrogen scale (SHE). The solutions were deoxygenated by continuously bubbling Ar through the electrolyte.

To determine the weight loss after exposure, the samples were first rinsed in pure water for 2 min to remove water soluble corrosion products and then treated for 4 min in saturated ammonium acetate solution, ultrasonically at ambient temperature, to dissolve the remaining corrosion products. The weight loss during corrosion product removal was measured and the average weight loss rate during the exposure period with chloride was determined.

Crystalline corrosion products were analysed by X-ray diffraction (XRD) using a MAC X-ray diffractometer equipped with a grazing incidence beam attachment. CuK_α radiation was used and the angle of incidence was 0.5°. The diffraction peaks of metallic zinc were used as an internal standard.

The corrosion products were qualitatively analysed by Fourier transform infrared (FTIR) spectroscopy (Bomem model DA8.2 SNV) in the reflection–absorption (RAS) mode from 500 to 4000 cm^{-1} with a 2 cm^{-1} resolution by using a globar as the infrared light source.

Surface analysis by X-ray photoelectron spectroscopy (XPS) is accomplished by irradiating a sample with monoenergetic soft X-ray and analysing the energy of the detected electrons. The XPS measurement were carried out on a Perkin–Elemer model PHI 1600 by using a single MgK_α X-ray operating at 250 W. The pressure in the vacuum chamber during analysis was 1×10^{-9} torr. The X-ray source was at an angle of 54.7°. An *in situ* 3 kV Ar^+ ion gun was applied to sputter the samples. Energy calibration was done by using the Au $4f_{7/2}$ peak at 83.8 eV. Based on the high-resolution spherical capacitor analyser (SCA), the energy resolution was 1.6 eV for the survey scan spectrum and 0.2 eV for the high resolution core level spectrum, respectively.

3. Results and discussion

3.1. *EIS of zinc in methanol/LiCl solution*

Figure 2 shows the typical EIS Nyquist plot for zinc in deaerated methanol doped with 0.003 M LiCl. It is well recognized that the polarization resistance (R_p) is inversely proportional to the corrosion rate. R_p which was graphically estimated from the diagram as $R_p = |Z(j\omega)|_{\omega\to 0} - |Z(j\omega)|_{\omega\to\infty}$, increased with immersion time in methanol, as shown in Figure 3. According to Banas et al. [30], small amounts of residual water in methanol stimulate the formation of a corrosion product layer which is responsible for the inhibition of zinc dissolution. However, the contribution to R_p from the surface layer formed during the EIS test is negligible due to the low formation rate.

The corrosion of zinc in the methanol/water/LiCl system has been studied by Banas et al. [30]. In deaerated methanol, the anodic and cathodic partial

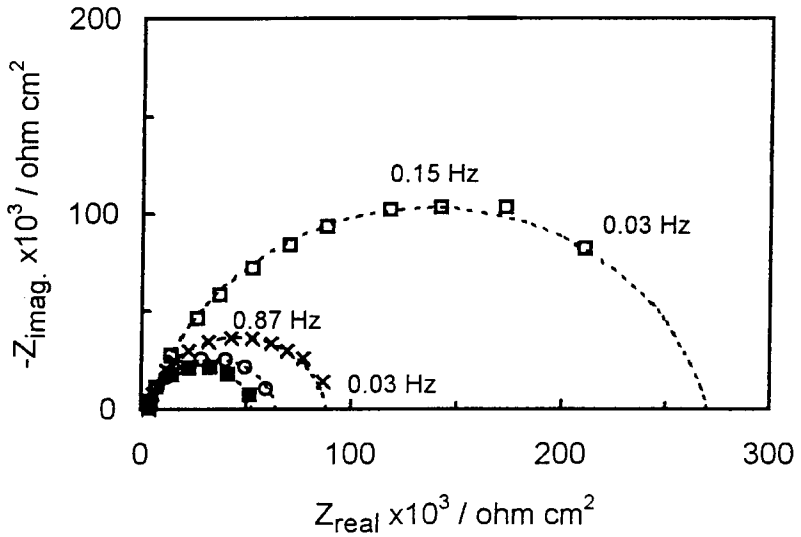

Fig. 2. Electrochemical impedance diagrams for Zn in the deaerated 0.003 M LiCl/methanol system as a function of the relative humidity of the atmosphere (containing 500 ppm CO_2) to which it was exposed to 72 h. RH: (■) 50%, (○) 85%, (×) 95% and (□) 100%.

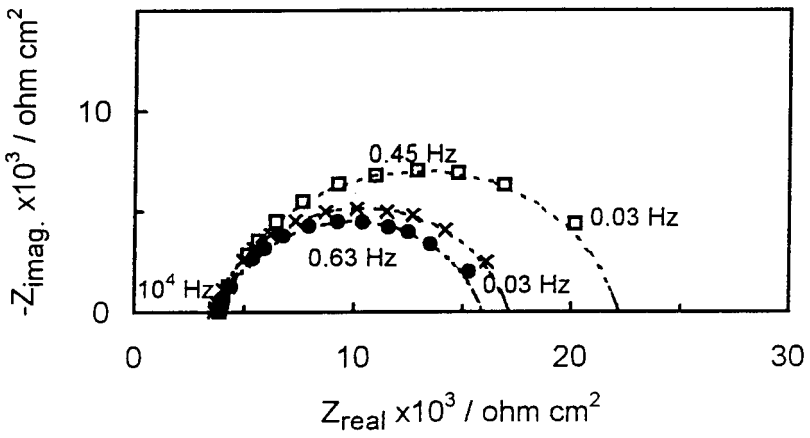

Fig. 3. Electrochemical impedance diagrams for Zn as a function of immersion time in the deaerated 0.003 M LiCl/methanol system. Immersion times: (●) null, (×) 5 min and (□) 15 min.

reactions are dissolution of zinc and evolution of hydrogen, respectively, as follows:

$$Zn \rightarrow Zn^{2+} + 2e^- \quad \phi^\circ_{25^\circ C} = -0.763\,V \tag{1a}$$

$$2CH_3OH + 2e^- \rightarrow 2CH_3O^- + H_2 \quad \phi^\circ_{25^\circ C} = -0.988\,V \tag{1b}$$

(The dissociation constant of methanol at 25 °C is 2×10^{-17} [31]). While atmospheric corrosion is more closely simulated by corrosion in an aqueous electrolyte than in methanol, the important differences can be reduced to the nature of the cathodic partial step (different proton donors) and the surface film formation capability. Corrosion in both aqueous electrolytes and methanol are cathodically controlled with a high hydrogen evolution overvoltage (Tafel slope = 120–250 mV (decade)$^{-1}$ [30]). In aqueous solutions, whether aerated or deaerated, oxide/hydroxide surface layers are formed. As the equilibrium potential of Zn/Zn^{2+} is highly negative, the reduction of water (H_2O/OH^-) can take place on the pure Zn surface. Hydroxide ions are a product of this reaction, which react with the Zn ions to form hydroxide surface films. This surface layer on zinc, formed in aqueous environments, inhibits further corrosion in methanol and, therefore, interferes with the measurements of interest on the corrosion product layer formed during the previous atmospheric exposure. In contrast, in nonaqueous methanol solutions, the metallic zinc surface remains free of additional corrosion product layers.

Under atmospheric exposure conditions, the corrosion of zinc is influenced by more complex environmental factors than in the methanol electrolyte. In methanol, the cathodic half reaction is hydrogen evolution (Equation 1(b)), whereas in atmospheric corrosion, oxygen reduction is more common. Under most atmospheric conditions, the moisture is slightly acidic, so the oxygen reduction occurs as follows:

$$\frac{1}{2}O_2 + 2H^+ + 2e^- \rightarrow H_2O \quad \phi^\circ_{25^\circ C} = 1.229\,V \tag{2}$$

However, in acid solutions, hydrogen evolution is also involved:

$$2H^+ + 2e^- \rightarrow H_2 \quad \phi^\circ_{25^\circ C} = 0\,V \tag{3}$$

Thus, if a corrosion layer results in cathodic polarization (high hydrogen overvoltage) in methanol, it has less influence on the cathodic reaction in practical atmospheric corrosion. But if a corrosion layer results in anodic polarization in methanol, it also provides corrosion resistance during atmospheric exposure since the anodic half reactions are the same (Equation 1(a)).

To estimate the correlation between R_p values obtained in methanol and the real corrosion rate, samples preexposed to atmospheres containing 350 ppm CO_2 and having various RH for 120 h were transferred into a 70% RH atmosphere containing 350 ppm CO_2 and examined with gravimetry and EIS in methanol. For the convenience of the weight-loss measurement, sodium chloride of concentration 1.5 μg cm^{-2} was added to each specimen surface to accelerate the corrosion during exposure to 70% RH. The weight loss and R_p in methanol were measured every 24 h up to the exposure period of 120 h and then the average values over 120 h of exposure were calculated, as shown in Figure 4. A linear correlation between the weight-loss rate and $1/R_p$ was found as follows:

$$\text{Weight-loss rate} = 1.49 \times 10^4\ (1/R_p) \tag{4}$$

The weight-loss rate and R_p are in units of mg cm^{-2} day^{-1} and Ω^{-1} cm^{-2}, respectively. Thus the agreement with the weight-loss rate confirmed that the EIS results were reliable and appropriate for study of atmospheric zinc corrosion. Since the weight loss during the initial stage of atmospheric zinc corrosion is too small to be measured, it is convenient to use R_p measured in methanol as an index of the real corrosion resistance.

3.2. *Effect of RH on the atmospheric zinc corrosion*

3.2.1. *EIS measurements in methanol*

Figure 5 shows R_p values obtained from impedance measurements in the 0.003 M LiCl/methanol system of zinc previously exposed to air containing 500 ppm CO_2 at various RHs for exposure periods up to 192 h. At higher RHs (95% and 100%), R_p increased monotonically with time and relative humidity (Figure 5(a)). At moderate RHs (50%, 70% RH and 85% RH), R_p reached a maximum value, then fell before finally slowly increasing again, as shown in Figure 5(b). The result

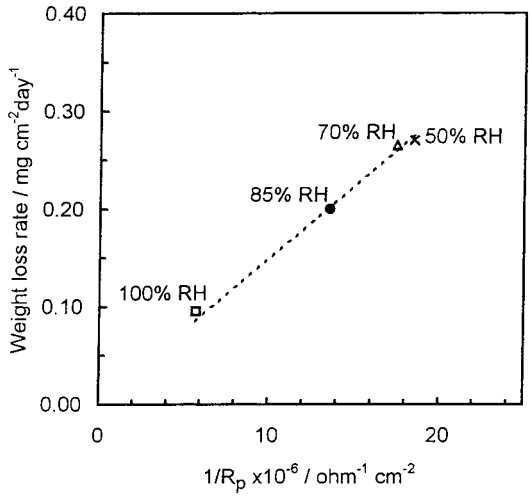

Fig. 4. The variation of weight loss rate as a function of $1/R_p$ measured in the 0.003 M LiCl/methanol system for zinc samples preexposed to atmospheres containing 350 ppm CO_2 with various relative humidities for 120 h and then exposed to a 70% RH atmosphere for 120 h with 1.5 μg cm^{-2} NaCl added. The dash line represents the linear correlation calculated using linear least squares fit (LLSF) technique.

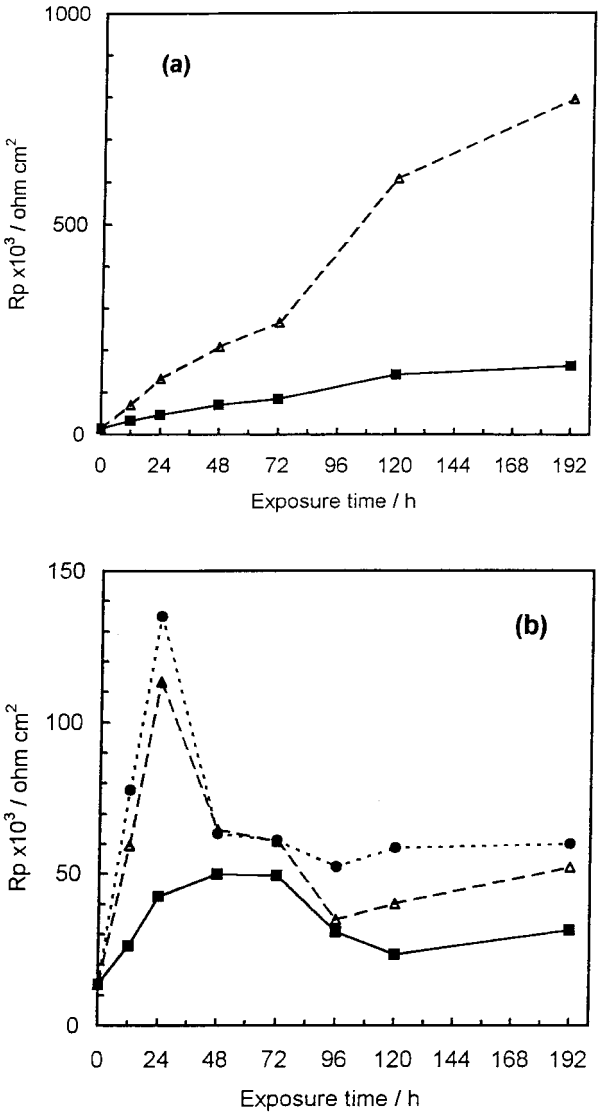

Fig. 5. R_p measured in the deaerated 0.003 M LiCl/methanol system as a function of the time that zinc samples were exposed to atmospheres containing 500 ppm CO_2 and having various relative humidities. (a) High relative humidities: (■) 95% and (△) 100%; (b) moderate relative humidities: (■) 50%, (△) 70% and (●) 85%.

implies a transition occurring in the early stages of corrosion. At the lowest RH tested (50%), R_p varied with time in this manner but did so more smoothly than at 70% and 85% RH. The value of R_p increased with RH at all exposure times.

3.2.2. *Characterization and analysis of the corrosion products*

The crystalline products were identified by grazing angle XRD and hydrozincite ($Zn_5(CO_3)_2(OH)_6$) and zincite (ZnO) were found only on the samples exposed to atmospheres of high RHs, as shown in Figure 6. On the samples exposed to atmospheres of moderate RHs, no crystalline corrosion product was found for exposure periods up to 192 h. The corrosion products may be of poor crystallinity or too thin to be detected. However, FTIR results revealed that carbonate appeared after 36 h exposure to air of 85% RH, as shown in Figure 7.

The corrosion product formed before 24 h exposure to air of moderate RH was examined by XPS. Figure 8(a) shows the survey scan spectrum taken from the sample previously exposed to air containing 500 ppm CO_2 at 85% RH for 20 h. Zn, O and C signals presented on the sample. Since detail examination by core-level spectra shows no signal, the presence of carbon may be due to atmospheric contamination rather than corrosion compounds, as shown in Figure 8(b). The O(1s) peak at 532.4 eV and the $Zn(2p_{3/2})$ peak at 1022.4 eV [32] indicated the presence of zinc hydroxide, $Zn(OH)_2$, on the surface, as shown in Figure 8(c) and 8(d). Zincite, identified by the O(1s) peak at 530.4 eV and the $Zn(2p_{3/2})$ peak at 1021.7 eV [33], was found the following compound under the surface zinc hydroxide layer. Therefore, the drop in R_p during exposure to air of moderate RH was attributed to the conversion of zincite to zinc hydroxy carbonate.

3.3. *Effect of CO_2 and O_2 concentration on atmospheric zinc corrosion*

3.3.1. *EIS measurements in methanol*

Zinc specimens were exposed to CO_2-free air, and air containing 40, 350, 500 and 1000 ppm CO_2 at 85% and 95% RH. Figure 9 shows R_p measured in the deaerated 0.003 M LiCl/methanol system, as a function of time in a 95% RH atmosphere. For 350 and 1000 ppm CO_2 concentrations at 95% RH, R_p increased monotonically with time, although values were somewhat lower at the lower CO_2 concentration. For a CO_2 concentration of zero or 40 ppm, R_p first increased and then leveled off. The R_p for 40 ppm CO_2 was even smaller than that for the CO_2-free environment.

The R_p values for zinc, previously exposed to various concentrations of CO_2 at 85% RH, and measured in the deaerated 0.003 M LiCl/methanol system are shown in Figure 10. In CO_2-free environments, the increase in R_p stopped after a brief rise. When the CO_2 concentration was increased to 40 ppm, a maximum value of R_p appeared after 24 h. If the CO_2 concentration was increased to 1000 ppm, the peak disappeared.

Figure 11 shows the R_p values for zinc, previously exposed to various concentrations of O_2 at 85% RH, CO_2-free atmosphere, and measured in the deaerated 0.003 M LiCl/methanol system. Without the presence of CO_2, oxygen shows no effect on the corrosion resistance of zinc exposed to atmospheres of moderate RHs.

3.3.2. *Characterization and analysis of the corrosion products*

The corrosion product for 20 h exposure to an 85% RH atmosphere containing 1000 ppm CO_2 was examined by XPS and carbonate was identified on the surface, as shown in Figure 12(a) [33]. Compared with Figure 8(c), zinc hydroxide and zincite became thicker as the CO_2 concentration increased, as shown in Figure 12(b).

The environmental factors, including RH, CO_2 and O_2, in the initial stages of corrosion may be explained as

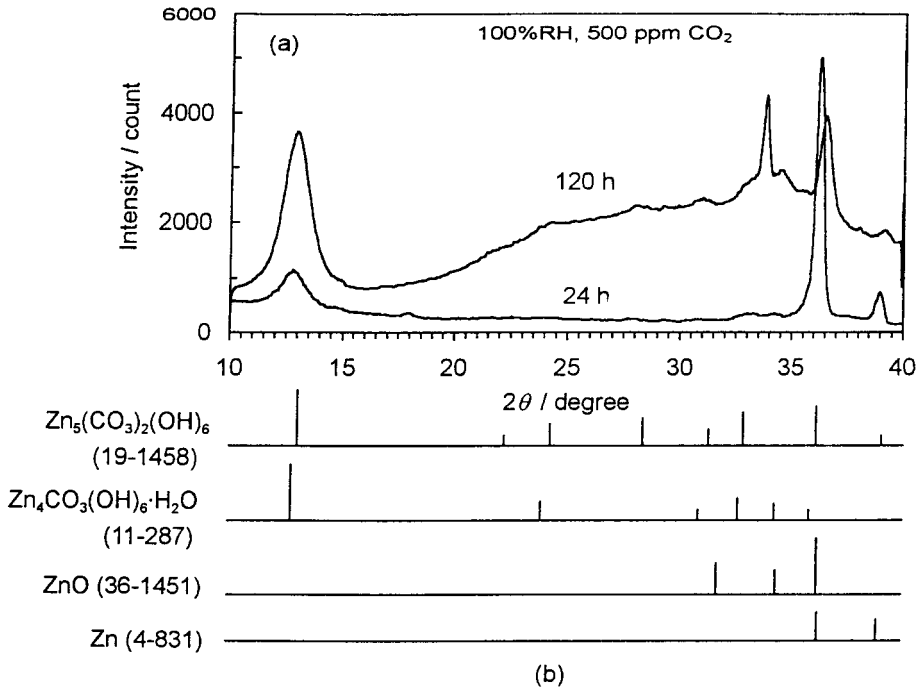

Fig. 6. (a) X-ray diffraction patterns obtained from zinc samples exposed to a 100% RH atmosphere containing 500 ppm CO_2 for 24 and 120 h. (b) The X-ray diffraction patterns and the JCPDS card numbers of the possible corrosion products.

follows: when zinc is exposed to high RH (≥95%) environments at 28 °C, the thickness of the adsorbed water layer is more than ten monolayers [34]. The behaviour of this layer of water approaches that of bulk solutions. The main role of the water layer on the metal surface is to provide a medium for the hydration and mobilization of ions. When CO_2 is present in the atmosphere, it dissolves in the surface electrolyte and acidifies the water in the form of carbonic acid, which is also the reactant of hydrozincite. Consequently, zincite and hydrozincite are the stable corrosion products. The formation of zincite and hydrozincite are accelerated with increasing RH and CO_2 concentration, simultaneously results in the increase of R_p.

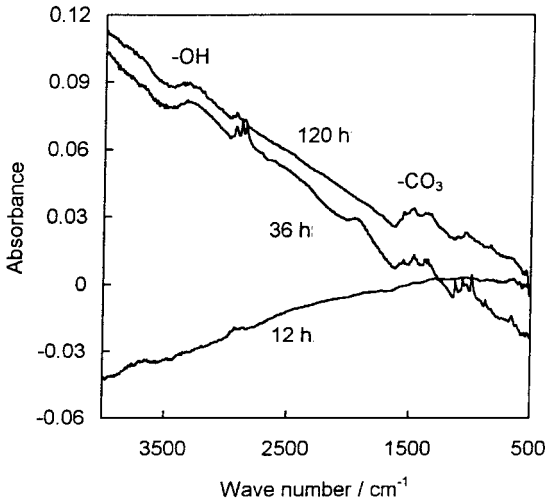

Fig. 7. FTIR spectra of zinc samples as a function of exposure time to an 85% RH atmosphere containing 500 ppm CO_2.

Zincite, rather than hydrozincite, exists in low-CO_2 or CO_2-free environments. In low CO_2 environment, any trace amount of CO_2 is insufficient for the formation of hydrozincite but acidifies the adsorbed electrolyte. Due to the acidification of the surface electrolyte, zincite becomes increasingly unstable with increasing CO_2 concentration in the exposure atmosphere, and R_p decreases. Therefore, the R_p value for an atmosphere of 95% RH containing 40 ppm CO_2 is lower than that for a CO_2-free environment.

In moderate RH (50–85%) environments at 28 °C, the thickness of the adsorbed water layer on a clean zinc surface is less than ten monolayers. This small amount of moisture is unlikely to have properties of bulk water and adsorption results in clustering, even on a homogeneous surface [35]. Although this thin water layer begins to fulfill the function of an electrolyte, the dielectric constant is low and hydration of ions is restricted. When CO_2 is present in the atmosphere, only a small amount of dissolved CO_2 is hydrated in the thin water layer on zinc to form carbonic acid. Thus, due to the small amount of carbonic acid, zincite is the stable corrosion product in this early stage [16]. The role of CO_2 in this stage is mainly to increase the conductivity of the surface adsorbed water layer. Meanwhile, R_p increases simultaneously. If CO_2 concentration is sufficiently high (e.g., 1000 ppm at 85% RH), the amount of dissolved CO_2 is able to facilitate the formation of zinc hydroxy carbonate in this stage. Furthermore, oxygen shows no effect on the formation of zincite since the equilibrium potential of zinc is sufficiently negative to reduce water directly.

When CO_2 is present, zinc hydroxy carbonate is formed after the initial formation of zincite. The reaction suggested by Graedel [1] is as follows:

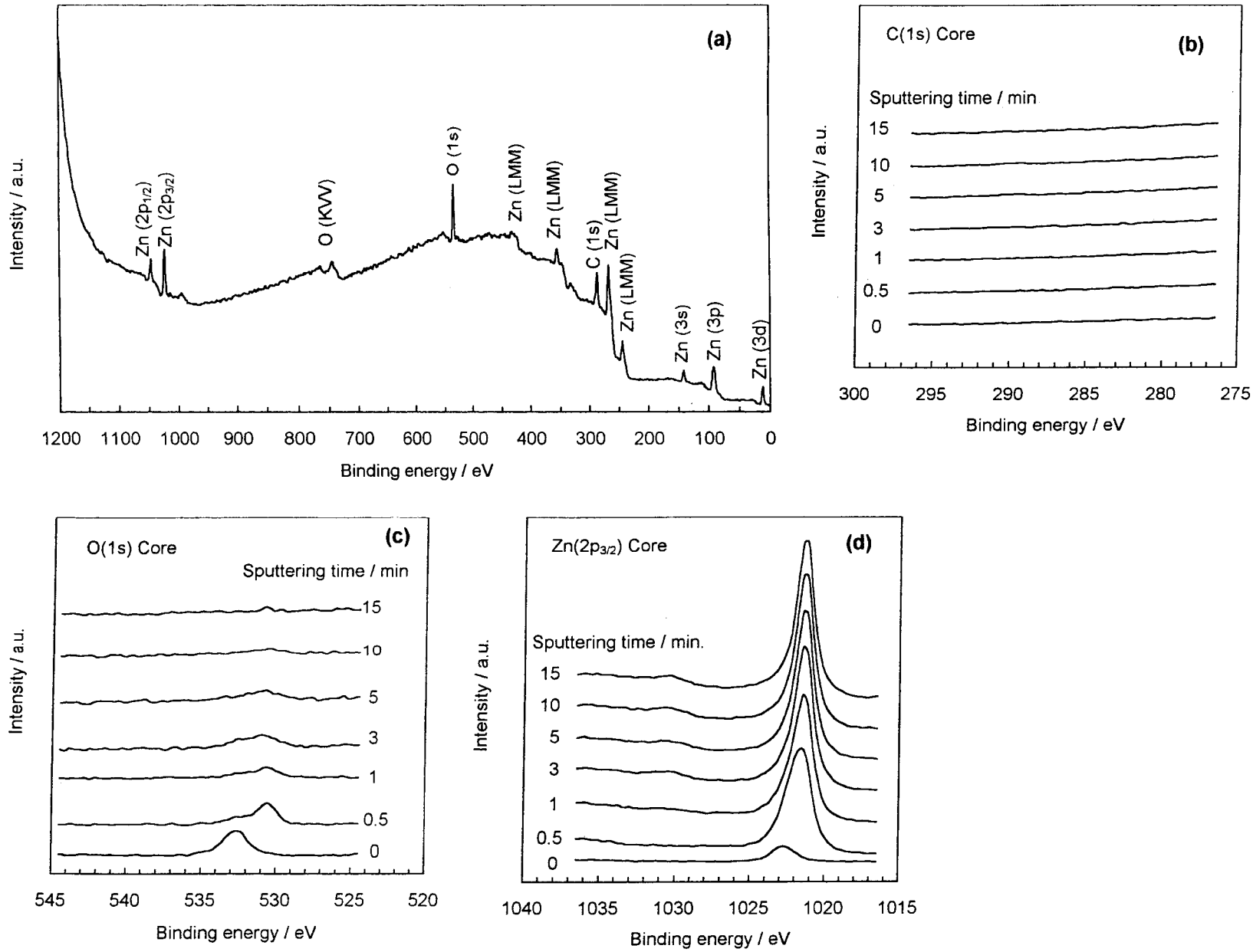

Fig. 8. XPS spectra of zinc samples exposed to an 85% RH atmosphere containing 500 ppm CO_2 for 20 h. (a) Survey spectrum, (b) high resolution core level spectrum of the C(1s) peak, (c) high resolution core level spectrum of the O(1s) peak and (d) high resolution core level spectrum of the $Zn(2p_{3/2})$ peak.

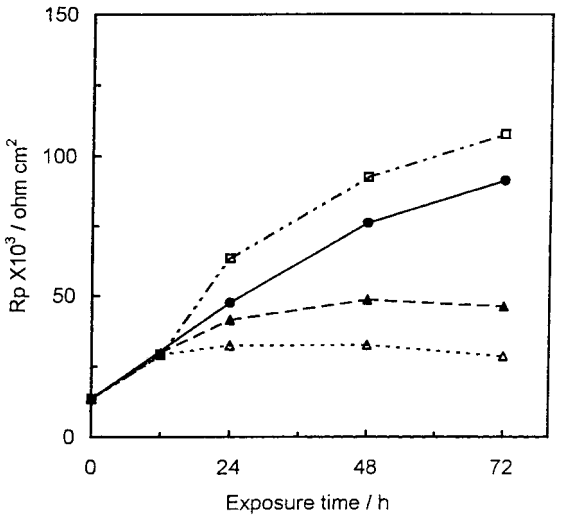

Fig. 9. R_p measured in the deaerated 0.003 M LiCl/methanol system as a function of the time that zinc was exposed to a 95% RH atmosphere containing various concentrations of CO_2. Key: (▲) CO_2-free, (△) 40 ppm, (●) 350 ppm and (□) 1000 ppm.

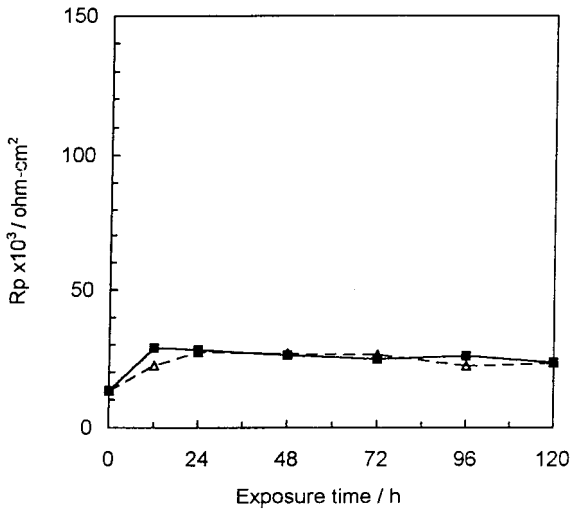

Fig. 11. R_p measured in the deaerated 0.003 M LiCl/methanol system as a function of the time that zinc was exposed to an 85% RH and CO_2-free atmosphere containing various concentrations of O_2. Key: (■) 18% O_2 and (△) 100% O_2.

$$Zn(OH)_{2(s)} + 4\,Zn^{2+} + 4\,OH^- + 2\,CO_3^{2-} \rightarrow Zn_5(CO_3)_2(OH)_6 \downarrow \quad (5)$$

According to the results for R_p obtained in methanol as a function of time, this conversion destroys the protectiveness of the zincite layer. Using electron diffraction, Anderson [36] studied the rate of formation of zinc carbonate layers and recognized the accelerating effect of water. In water, a layer of carbonate was formed after only 30 s of immersion. In air, at 75% RH, the zinc surface was covered by carbonate after one day. When the samples were exposed to air with 33% RH, the carbonate layer first appeared after two days and completely covered the surface after 14 days. These

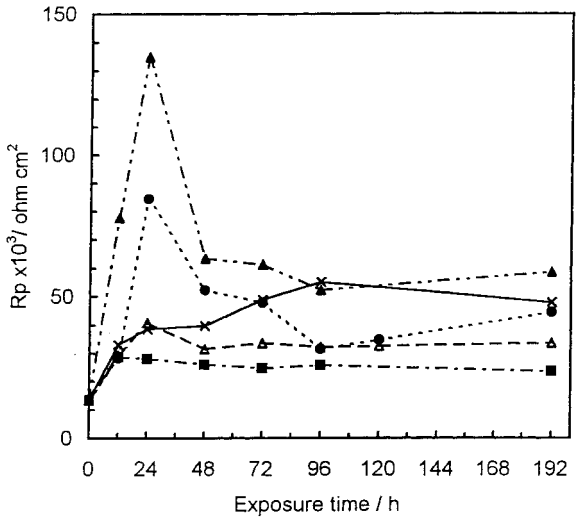

Fig. 10. R_p measured in the deaerated to 0.003 M LiCl/methanol system as a function of the time that zinc was exposed to an 85% RH atmosphere containing various concentrations of CO_2. Key: (■) CO_2-free, (△) 40 ppm, (●) 350 ppm, (▲) 500 ppm and (×) 1000 ppm.

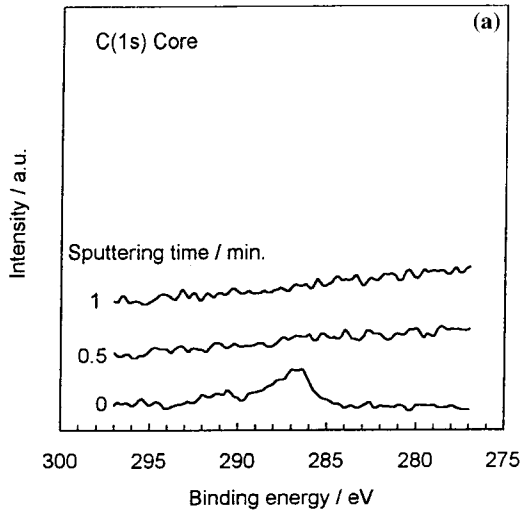

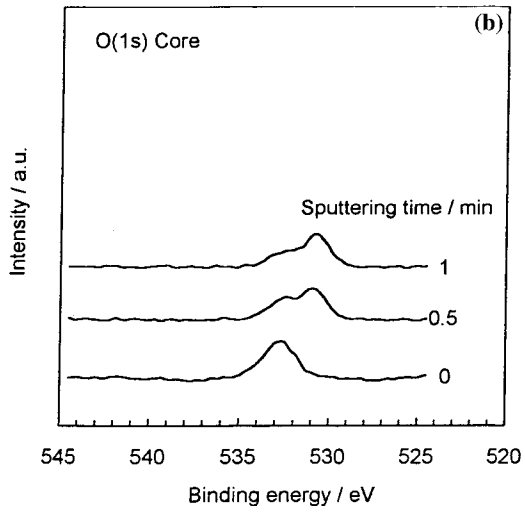

Fig. 12. XPS spectra of zinc samples exposed to an 85% RH atmosphere containing 1000 ppm CO_2 for 20 h. (a) High resolution core level spectrum of the C(1s) peak and (b) high resolution core level spectrum of the O(1s) peak.

time periods are in good agreement with the time for zinc, exposed to moderate RHs, to reach a maximum value of R_p in the present study. The increase in CO_2 concentration from 40 to 500 ppm does not reduce the time for achievement of the maximum value of R_p but only raises the maximum value of R_p. This implies that the adsorbed electrolyte layer thickness, rather than the CO_2 and O_2 concentrations, is the crucial factor in atmospheric corrosion at moderate RHs. After the fall in R_p, the zinc hydroxy carbonate grows and provides corrosion protection.

4. Conclusions

(i) The *ex-situ* EIS method in methanol has been shown to characterize the protectiveness of the corrosion products formed during the initial stage of atmospheric zinc corrosion. The weight-loss rate was found in a linear correlation with $1/R_p$ measured in methanol. Calibration using data from weight-loss experiments in the initial stages of corrosion shows that the electrochemical technique is suitable for estimating short-term variations in corrosion rates.

(ii) At high RH (95% and 100%) in the presence of CO_2, zincite and hydrozincite are the corrosion products and their formation is accelerated with increasing RH and CO_2 concentration. Therefore, the R_p value increases. Since the adsorbed electrolyte acts as bulk solution, the role of CO_2 is mainly in supplying the reactant of hydrozincite. In low-CO_2 or CO_2-free environments, the trace amounts of CO_2 are insufficient for the formation of hydrozincite but cause acidification of the adsorbed electrolyte. Hence, zincite becomes increasingly unstable with increasing CO_2 concentration in the exposure atmosphere and R_p decreases.

(iii) At moderate RH (50%, 70% and 85%) in the presence of CO_2, zincite is the first corrosion product. The role of CO_2 in this stage is mainly in increasing the conductivity of the adsorbed surface water layer. Hydrozincite forms after the initial formation of zincite and this conversion results in the drop in R_p. The increase in RH greatly reduces the time period for zinc to reach a maximum value of R_p but the increase in CO_2 concentration only affects the maximum value of R_p. The adsorbed electrolyte layer thickness is the crucial factor in atmospheric corrosion at moderate RHs. In high CO_2 environments (1000 ppm), zincite and hydrozincite forms together and no peak of R_p is found.

Acknowledgements

Financial support of this work by the National Science Council of the Republic of China under contract NSC-85-2216-E-007-012 is gratefully acknowledged.

References

1. T.E. Graedel, *J. Electrochem. Soc.* **136** (1989) 193C.
2. J.M. Costa and M. Vilarrasa, *Brit. Corros. J.* **28** (1993) 117.
3. I. Odnevall and C. Leygraf, *in* W.W. Kirk and H.H. Lawson (Eds), 'Atmospheric Corrosion', ASTM STP 1239, (American Society for Testing and Materials, Philadelphia, PA, 1995), p. 215.
4. S. Oesch and M. Faller, *Corros. Sci.* **39** (1997) 1505.
5. D.R. Flinn, S.D. Cramer, J.P. Carter, D.M. Hurwitz and P.J. Linstrom, *in* R. Baboian, (Ed.), 'Materials Degradation Caused by Acid Rain', ACS Symposium 318, (American Chemical Society, Washington, DC, 1986), p. 119.
6. J.J. Friel, *Corrosion* **42** (1986) 422.
7. J.E. Svensson and L.G. Johansson, *Corros. Sci.* **34** (1993) 721.
8. J.E. Svensson and L.G. Johansson, *J. Electrochem. Soc.* **143** (1996) 51.
9. S. Cramer, J.P. Carter, P.J. Linstrom and D.R. Flinn, *in* S.W. Dean and T.S. Lee (Eds.), 'Degradation of Metals in the Atmosphere', ASTM STP 965 (American Society for Testing and Materials, Philadelphia, PA, 1988), p. 229.
10. V. Kucera and E. Mattsson, *in* F. Mansfeld (Ed.), 'Corrosion Mechanisms', (Marcel Dekker, New York, 1987), p. 211.
11. J.H. Wang, F.I. Wei and H.C. Shih, *Corrosion* **52** (1996) 600.
12. J.H. Wang, F.I. Wei and H.C. Shih, *Corrosion* **52** (1996) 900.
13. H.H. Lawson, *in* B.C. Syrett (Ed.), 'Corrosion Testing Made Easy, Volume 4: Atmospheric Corrosion Testing Methods', (NACE International, Houston, TX, 1995), p. 23.
14. F. Mansfeld, *in* W. Ailor (Ed.), 'Atmospheric Corrosion', (J. Wiley & Sons, New York, 1982), p. 139.
15. W. Feitknecht, *Chem. Ind.* **5** (1959) 1102.
16. R. Grauer and W. Feitknecht, *Corros. Sci.* **7** (1967) 629.
17. T. Falk, J.E. Svensson and L.G. Johansson, *J. Electrochem. Soc.* **145** (1998) 39.
18. I. Odnevall and C. Leygraf, *Corros. Sci.* **34** (1993) 1213.
19. R.E. Lobnig, D.J. Siconolfi, L. Psota-Kelty, G. Grundmeir, R.P. Frankenthal, M. Stratmann and J.D. Sinclair, *J. Electrochem. Soc.* **143** (1996) 1539.
20. J.C. Oung and H.C. Shih, *Corros. Prevent. Control* **44** (1997) 173.
21. C. Fiaud, M. Keddam, A. Kadri and H. Takenouti, *Electrochim. Acta* **32** (1987) 445.
22. M. Keddam, A. Hugot-Le-Goff, H. Takenouti, D. Thierry and M. C. Arevalo, *Corros. Sci.* **33** (1992) 1243.
23. X.G. Zhang and E.M. Valeriote, *in* W.W. Kirk and H.H. Lawson (Eds), 'Atmospheric Corrosion', ASTM STP 1239 (American Society for Testing and Materials, Philadelphia, PA, 1995), p. 230.
24. A. Nishikata, Y. Ichihara and T. Tsuru, *Corros. Sci.* **37** (1995) 897.
25. A. Nishikata, Y. Ichihara, Y. Hayashi and T. Tsuru, *J. Electrochem. Soc.* **144** (1997) 1244.
26. N.D. Tomashov, *Corrosion* **20** (1964) 7t.
27. H.C. Shih, J.C. Oung, J.T. Hsu, J.Y. Wu and F.I. Wei, *Mater. Chem. Phys.* **37** (1994) 230.
28. L. Bai and B.E. Conway, *J. Electrochem. Soc.* **137** (1990) 3737.
29. G. Nonhebel and H. Hartley, *Phil. Mag.* **50** (1923) 729.
30. J. Banas, K.G. Schütze and E. Heitz, *J. Electrochem. Soc.* **133** (1986) 253.
31. W.F.K. Wynne-Jones, *J. Phys. Chem.* **31** (1927) 1657.
32. D. Persson and C. Leygraf, *J. Electrochem. Soc.* **142** (1995) 1459.
33. 'NIST X-ray Photoelectron Spectroscopy Database', NIST Standard Reference Database 20 (US Department of Commerce, Gaithersburg, MD, 1989).
34. P.V. Strekalov, V.V. Agafonov and Yu. N. Mikhailovs.kii, *Prot. Met.* **8** (1972) 521.
35. P.B.P. Phipps and D.W. Rice, *in* G.R. Brubaker and P.B.P. Phipps (Eds), 'Corrosion Chemistry', ACS Symposium Series Vol. 89 (American Chemical Society, 1979), p. 235.
36. E.A. Anderson and M.L. Fuller, *Met. Alloys* **10** (1939) 282.